International Journal of Basic and Applied Sciences, 14 (8) (2025) 15-32

International Journal of Basic and Applied Sciences

Website: www.sciencepubco.com/index.php/IJBAS
https://doi.org/10.14419/vm282t91
Research paper

Topological Codescriptors for Predicting Lithium Clusters Binding Energy and Comparative Topological Study of Hexagonal and Rectangular Porous Nano Graphene

Parvez Ali [1] *, Syed Ajaz K. Kirmani [2], Omar M. A. Alhabib [1], Sultan K. AlSulaim [1]

[1] Department of Mechanical Engineering, College of Engineering, Qassim University, Buraydah,51452, Saudi Arabia
[2] Department of Electrical Engineering, College of Engineering, Qassim University, Buraydah,51452, Saudi Arabia
**Corresponding author E-mail: p.ali@qu.edu.sa*

Received: September 27, 2025, Accepted: November 13, 2025, Published: December 4, 2025

Abstract

The stability of lithium-ion batteries is heavily impacted by the uncontrolled formation of lithium dendrites, which pose a significant safety risk. The chemical and structural properties of small lithium clusters are critical to controlling this phenomenon and improving electrode potential. The use of traditional techniques, including large-scale experiments and DFT calculations, provides useful insights but is often hindered by high costs and long timeframes. This study addresses this challenge by proposing a novel approach using the CoM Polynomial, a new tool in chemical graph theory. We construct molecular graphs for minimized lithium cluster structures from previous studies and utilize the CoM Polynomial to generate codescriptors for each cluster. This approach extracts significant structural information, enabling a more robust analysis of cluster properties. Curvilinear regression analysis then identifies highly significant regression equations and informative codescriptors, revealing strong relationships between these codescriptors and the binding energy of the clusters. Furthermore, lithium metal holds tremendous promise as an anode material for lithium-ion batteries but faces challenges like dendritic growth and unstable solid electrolyte interphase formation. Researchers are exploring porous graphene frameworks as a potential solution. In this vein, we investigated the molecular structure of hexagonal and rectangular porous nano graphene using the CoM Polynomial to obtain analytical expressions for their topological codescriptors. This study offers insights that can help researchers improve the safety, efficiency, and sustainability of energy storage devices by better understanding the properties of lithium clusters and porous nano graphene.

Keywords: *CoM Polynomial; Lithium Clusters; Binding Energy; Hexagonal and Rectangular Porous Nano Graphene Structures.*

1. Introduction

The scientific community is currently captivated by the exceptional properties and applications of clusters and nanostructures in a variety of cutting-edge technologies. Clusters, which act as a bridge between individual atoms and bulk materials, are vital for exploring the link between structure and function. They have a wide range of uses, from chemical sensing and optoelectronics to biomedicine, catalysis, and energy research [1-6].

Of particular importance are small metal clusters, especially lithium clusters, which are a prevalent topic due to their role in various processes, including their presence on the anodes of lithium-ion batteries (LIBs) [7], [8]. While LIBs are highly effective for energy storage, a major safety issue arises with the use of lithium metal anodes: the uncontrolled formation of lithium (Li) dendrites [9]. These dendrites are a result of the clumping of Li atoms and can compromise battery integrity. According to first-principles DFT calculations by Kushwaha and Nayak [10], dendrite growth is tied to the average binding energy per atom of the cluster (BE/n). Furthermore, a cluster's stability depends on whether it contains an odd or even number of atoms, with even-numbered clusters generally being more stable and exhibiting an even-odd oscillation in binding energy as the number of atoms increases [11].

Understanding the binding energy of lithium clusters is critical for revealing their stability, reactivity, and electronic behavior, which is essential for developing and refining new materials. However, determining this energy presents significant hurdles, whether through time-consuming laboratory experiments or computationally intensive quantum chemical calculations.

Porous Nano Graphene (PNG) has recently emerged as a promising anode material because its unique architecture can help mitigate lithium dendrite formation [12-14]. These porous nano graphene materials have numerous benefits, including chemical stability, low density, and high thermal and electrical conductivity, and they can be fabricated with a large surface area and customizable pore sizes [15], [16]. PNG

can be categorized by pore size, and this size has a significant impact on the material's performance. For instance, a study found that while mesoporous PNG enhanced coulombic efficiency, microporous PNG caused a substantial drop, suggesting that pore size plays a role in dendrite growth. Scientists have employed different methods to create PNG with specific structural attributes [17], [18]. Bieri et al., for example, pioneered a technique to convert graphene into porous graphene by precisely removing phenyl rings [19]. Subsequent research has shown how to create these structures with controlled on-surface synthesis [20-26].

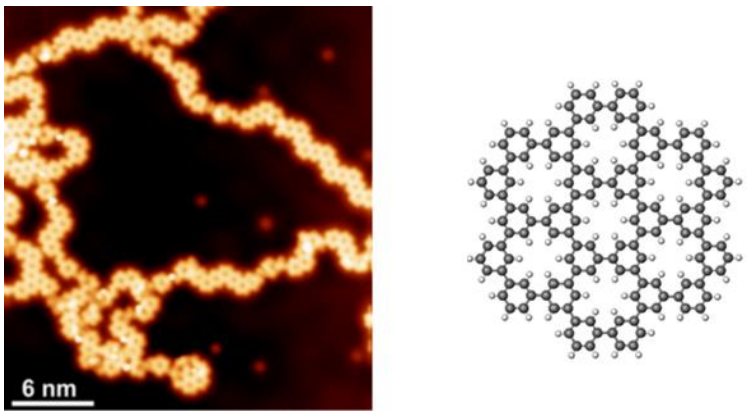

Fig. 1: STM Image Showing the Formation of PNG with Periodic Pores and Structure of PNG [22].

A thorough investigation of both lithium clusters and PNG is vital for making strides in various technological areas. Analyzing lithium cluster properties provides insights into foundational concepts like cluster formation and stability, which in turn aid in the design of nano-materials and enhance battery technology. Researchers often use Quantitative Structure-Property Relationships (QSPR) to predict a material's properties based solely on its chemical structure, which eliminates the need for physical synthesis and testing. A key element of this approach is chemical graph theory, which converts chemical structures into molecular graphs and uses topological descriptors to represent them as numerical values [27], [28].

The field of chemical graph theory has seen several innovations since Harold Wiener's initial work on the Wiener index [29]. This led to the creation of the M-Polynomial, a tool for deriving numerous descriptors at once, and more recently, the NM-Polynomial and the CoM Polynomial [30-32]. Past research has applied these methods to porous graphene and polyphenylene honeycomb structures, as well as to lithium clusters [33-40].

Motivated by the pivotal role of these materials in energy storage devices, this article has two main goals. First, we present an efficient new method for calculating the binding energy of lithium clusters. Second, we fill a gap in the existing literature by computing the CoM Polynomial of hexagonal and rectangular porous nano graphene structures.

Throughout this paper, we represented G_{MG} as a molecular graph with $|V_{MG}|$ and $|E_{MG}|$ as the number of vertices and edges in G_{MG} . The complement of G_{MG} is denoted as $\overline{G}_{MG}$ such that $uv \in \overline{G}_{MG}$ if $uv \notin G_{MG}$ and $d(u)$ denotes the degree of a vertex as the number of vertices adjacent to the vertex $u \in V_{MG}$. The CoM Polynomial for G_{MG} is defined as

$$CoM(G_{MG}; x, y) = \overline{M}(G_{MG}; x, y) = \sum_{i \le j} \overline{m}_{ij}(G_{MG}) x^i y^j \quad (1)$$

Where,

$n_i = |V_i|$ for $V_i = \{v \in V_{MG} | d_{G_{MG}}(v) = i\}$,

$m_{ij} = |E_{ij}|$ for $E_{ij} = \{uv \in E_{MG} | d_{G_{MG}}(u) = i \text{ and } d_{G_{MG}}(v) = j\}$

$\overline{m}_{ij} = |\overline{E}_{ij}|$ for $\overline{E}_{ij} = \{uv \in E_{M\overline{G}} | d_{G_{MG}}(u) = i \text{ and } d_{G_{MG}}(v) = j\}$

and from [41] $\overline{m}_{ij}$ can be found as

$$\overline{m}_{ij} = |\overline{E}_{ij}| = \begin{cases} \frac{n_i(n_i-1)}{2} - m_{ii} \text{ for } i = j \\ n_i n_j - m_{ij} \text{ for } i < j \end{cases} \quad (2)$$

From (1), several codescriptors can be obtained as below.

First Zagreb codescriptor: $\overline{M}_1(G_{MG}) = \sum_{uv \notin E_{MG}} (d(u) + d(v))$

Second Zagreb codescriptor: $\overline{M}_2(G_{MG}) = \sum_{uv \notin E_{MG}} d(u)d(v)$

Second modified Zagreb codescriptor: $m\overline{M}_2(G_{MG}) = \sum_{uv \notin E_{MG}} \frac{1}{d(u)d(v)}$

Redefined third Zagreb codescriptor: $\overline{ReZG_3}(G_{MG}) = \sum_{uv \notin E_{MG}} d(u)d(v)(d(u) + d(v))$

Forgotten topological codescriptor: $\overline{F}(G_{MG}) = \sum_{uv \notin E_{MG}} (d^2(u) + d^2(v))$

Randić codescriptor: $\overline{R}_k(G_{MG}) = \sum_{uv \notin E_{MG}} (d(u)d(v))^k$

Inverse Randić codescriptor: $\overline{RR}_k(G_{MG}) = \sum_{uv \notin E_{MG}} \frac{1}{(d(u)d(v))^k}$

Symmetric Division codescriptor: $\overline{SDD}(G_{MG}) = \sum_{uv \notin E_{MG}} \frac{\chi^2(u)+\chi^2(v)}{d(u)d(v)}$

Harmonic codescriptor: $\overline{H}(G_{MG}) = \sum_{uv \notin E_{MG}} \frac{2}{d(u)+d(v)}$

Inverse sum indeg codescriptor: $\overline{I}(G_{MG}) = \sum_{uv \notin E_{MG}} \frac{d(u)d(v)}{(d(u)+d(v))}$

Augmented Zagreb codescriptor: $\overline{A}(G_{MG}) = \sum_{uv \notin E_{MG}} \left\{\frac{d(u)d(v)}{d(u)+d(v)-2}\right\}^3$

Also, derivation from $CoM(G_{MG}; x, y) = f(x, y)$ For the above codescriptors, required following are required:

$(D_x + D_y)(f(x, y))_{x=y=1}$

$\left(D_x D_y\right)\left(f(x, y)\right)_{x=y=1}$

$\left(S_x S_y\right)\left(f(x, y)\right)_{x=y=1}$

$D_x D_y\left(D_x + D_y\right)\left(f(x, y)\right)_{x=y=1}$

$\left({D_x}^2 + {D_y}^2\right)\left(f(x, y)\right)_{x=y=1}$

$\left({D_x}^k {D_y}^k\right)\left(f(x, y)\right)_{x=y=1}$

$\left({S_x}^k {S_y}^k\right)\left(f(x, y)\right)_{x=y=1}$

$(D_x S_y + S_x D_y)(f(x, y))_{x=y=1}$

$(2S_x J)\left(f(x, y)\right)_{x=1}$

$\left(S_x J D_x D_y\right)\left(f(x, y)\right)_{x=1}$

$\left({S_x}^3 Q_{-2} J {D_x}^3 {D_y}^3\right)\left(f(x, y)\right)_{x=1}$

Where

$D_x = x\left(\frac{\partial(f(x,y))}{\partial x}\right), D_y = y\left(\frac{\partial(f(x,y))}{\partial y}\right), S_x = \int_0^x \frac{f(t,y)}{t} dt,$

$S_y = \int_0^y \frac{f(x,t)}{t} dt, J\left(f(x, y)\right) = f(x, x),\ Q_k\left(f(x, y)\right) = x^k f(x, y)$

The remainder of this paper is structured as follows. Section 2 examines the correlation between the binding energy of lithium clusters and their associated topological codescriptors. Section 3 provides a detailed topological analysis of both rectangular and hexagonal porous nano-graphene structures and presents a numerical comparison of their descriptor values, including a dedicated comparative evaluation of HPG versus RPG (Section 3.3). Section 4 contains the Discussion, beginning with an interpretation of the role of topological codescriptors in predicting binding energy (Section 4.1), followed by a critical examination of model limitations and extrapolation considerations (Section 4.2), and finally an outlook on future directions (Section 4.3). The future work is organised into three thematic streams: strengthening and generalising the lithium-cluster modelling framework (Section 4.3.1), expanding the descriptor family (Section 4.3.2), and extending the porous-graphene topology theory (Section 4.3.3). The paper concludes with a summary of the key findings in Section 5.

2. Lithium Cluster Binding Energy: An Analysis of Its Relationship with Topological Codescriptors

To accelerate material discovery and optimize design processes, researchers rely heavily on molecular descriptors for property prediction. As a cost-effective and time-saving alternative to traditional methods, these descriptors are particularly valuable in the early stages, enabling researchers to focus on promising materials and tailor synthesis conditions to achieve desired properties. This section investigates the predictive capabilities of codescriptors derived from the CoM Polynomial. To evaluate their effectiveness in property prediction and assess their potential for broader application, we constructed molecular graphs from the most stable lithium cluster structures, as detailed in [39] and shown in Figure 2.

$Open(\mathrm{Li_4}: \mathrm{BE} = 0.66)$

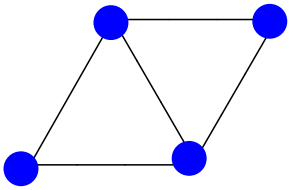

$\mathrm{CoM}(\mathrm{Li_4}; x, y) = x^2y^2$

$(\mathrm{Li_5}: \mathrm{BE} = 0.72)$

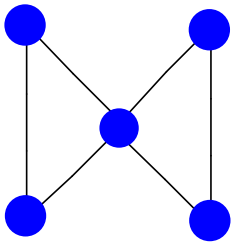

$\mathrm{CoM}(\mathrm{Li_5}; x, y) = 4x^2y^2$

$(\mathrm{Li_6}: \mathrm{BE} = 0.80)$

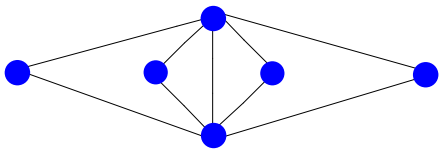

$\mathrm{CoM}(\mathrm{Li_6}; x, y) = 6x^2y^2$

$(\mathrm{Li_7}: \mathrm{BE} = 0.86)$

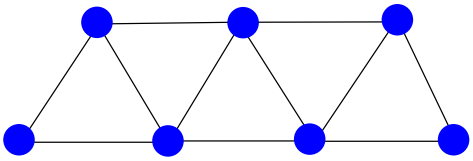

$\mathrm{CoM}(\mathrm{Li_7}; x, y) = x^2y^2 + 2x^2y^3 + 4x^2y^4 + x^3y^3 + 2x^3y^4$

$(\mathrm{Li_8}: \mathrm{BE} = 0.88)$

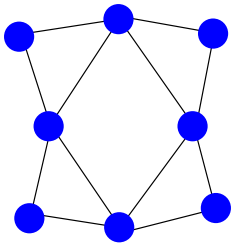

$\mathrm{CoM}(\mathrm{Li_8}; x, y) = 6x^2y^2 + 8x^2y^4 + 2x^4y^4$

$(\mathrm{Li_9}: \mathrm{BE} = 0.89)$

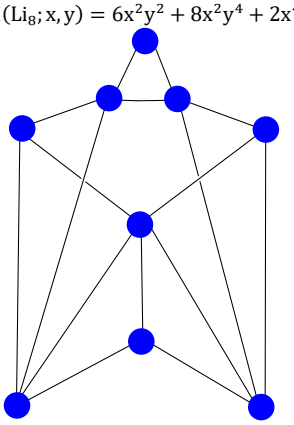

$\mathrm{CoM}(\mathrm{Li_9}; x, y) = 4x^2y^3 + 2x^2y^4 + 3x^3y^3 + 8x^3y^4 + 3x^4y^4$

$(Li_{10}: BE = 0.91)$

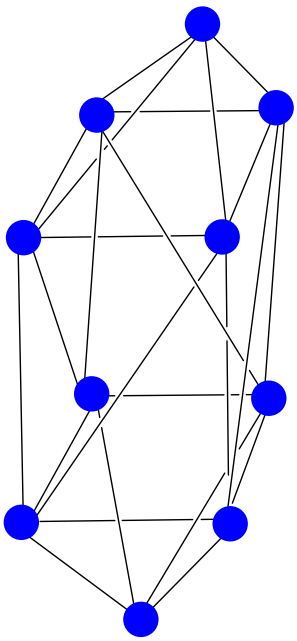

$CoM(Li_{10}; x, y) = x^4y^4 + 8x^4y^5 + 12x^5y^5$

Fig. 2: Minimized Structures of Li_N $(N = 4 - 10)$ with Their Binding Energies Obtained by Density Functional Method and Their Corresponding Molecular Graphs with CoM Polynomial.

Using the edge partition method, we computed the CoM Polynomial for the molecular graphs in Figure 2, as exemplified by the lithium cluster (Li_7) , whose graph contains 11 edges and 7 vertices. The edge set of (Li_7) classified into 4 classes as below:

$m_{23} = |E_{23}| = 2, m_{24} = |E_{24}| = 2, m_{34} = |E_{34}| = 4, m_{44} = |E_{44}| = 3.$

Now (Li_7) vertex set classified as $n_2 = |V_2| = 2, n_3 = |V_3| = 2, n_4 = |V_4| = 3.$

By 2, we have $\bar{m}_{22} = \frac{(n_2)(n_2-1)}{2} - m_{22} = 1$, $\bar{m}_{23} = n_2n_3 - m_{23} = 2$, $\bar{m}_{24} = n_2n_4 - m_{24} = 4$, $\bar{m}_{33} = \frac{(n_3)(n_3-1)}{2} - m_{33} = 1$, and $\bar{m}_{34} = n_3n_4 - m_{34} = 2$

Now by (1), we have

$$CoM(G_{MG}; x, y) = \sum_{i \le j} \bar{m}_{ij}(G_{MG}) x^i y^j$$

$CoM(Li_7; x, y) = \sum_{2\le2} \bar{m}_{23}\, x^2y^2 + \sum_{2\le3} \bar{m}_{23}\, x^2y^3 + \sum_{2\le4} \bar{m}_{24}\, x^2y^4 + \sum_{3\le3} \bar{m}_{33}\, x^3y^3 + \sum_{3\le4} \bar{m}_{34}\, x^3y^4$

$CoM(Li_7; x, y) = x^2y^2 + 2x^2y^3 + 4x^2y^4 + x^3y^3 + 2x^3y^4$

Also $f(x, y) = CoM(Li_7; x, y) = x^2y^2 + 2x^2y^3 + 4x^2y^4 + x^3y^3 + 2x^3y^4$

Then

- $D_x f(x, y) = 2x^2y^2 + 4x^2y^3 + 8x^2y^4 + 3x^3y^3 + 6x^3y^4.$
- $D_y f(x, y) = 2x^2y^2 + 6x^2y^3 + 16x^2y^4 + 3x^3y^3 + 8x^3y^4.$
- $(D_x + D_y)(f(x, y)) = 4x^2y^2 + 10x^2y^3 + 24x^2y^4 + 6x^3y^3 + 14x^3y^4.$
- $D_yD_x(f(x, y)) = 4x^2y^2 + 12x^2y^3 + 32x^2y^4 + 9x^3y^3 + 24x^3y^4.$
- $(D_x^2 + D_y^2)(f(x, y)) = 8x^2y^2 + 26x^2y^3 + 80x^2y^4 + 18x^3y^3 + 50x^3y^4.$
- $D_x{}^k D_y{}^k(f(x, y)) = (2^k2^k)\, x^2y^2 + (2^k3^k)2x^2y^3 + (2^k4^k)4x^2y^4 + (3^k3^k)x^3y^3 + (3^k4^k)2x^3y^4$
- $D_xD_y(D_x + D_y)(f(x, y) = 16x^2y^2 + 60x^2y^3 + 192x^2y^4 + 54x^3y^3 + 168x^3y^4.$
- $S_xS_y(f(x, y)) = \frac{1}{(4)}x^2y^2 + \frac{1}{(3)}x^2y^3 + \frac{1}{(2)}x^2y^4 + \frac{1}{(9)}x^3y^3 + \frac{1}{(6)}x^3y^4.$
- $(S_yD_x + S_xD_y)(f(x, y)) = 2x^2y^2 + \frac{13}{(3)}x^2y^3 + 10x^2y^4 + 2x^3y^3 + \frac{25}{(6)}x^3y^4.$

- $S_x\, J\, D_y D_x\big(f(x,y)\big) = x^4 + \frac{53}{6}x^6 + \frac{24}{7}x^7.$
- $S_x{}^3 Q_{-2}\, J\, D_x{}^3 D_y{}^3\big(f(x,y)\big) = 8x^2 + 16x^3 + \frac{2777}{64}x^4 + \frac{3456}{125}x^5.$

Topological codescriptors for lithium cluster such as $\overline{M}_1(Li), \overline{M}_2(Li), m\overline{M}_2(Li), \overline{ReZG_3}(Li), \overline{F}(Li), \overline{R}_{-\frac{1}{2}}(Li), \overline{SDD}(Li), \overline{H}(Li), \overline{I}(Li)$ and $\overline{A}(Li)$ obtained from the CoM Polynomial of Li_7 given below

1) $\overline{M}_1(Li_7) = \big(D_x + D_y\big)f(x,y)\big|_{x=y=1} = 58$

2) $\overline{M}_2(Li_7) = D_x D_y f(x,y)\big|_{x=y=1} = 81$

3) $m\overline{M}_2(Li_7) = S_x S_y f(x,y)\big|_{x=y=1} = 1.3611$

4) $\overline{ReZG_3}(Li_7) = D_x D_y (D_x + D_y) f(x,y)\big|_{x=y=1} = 490$

5) $\overline{F}(Li_7) = (D_x^2 + D_y^2)(f(x,y))\big|_{x=y=1} = 182$

6) $\overline{R}_{-1/2}(Li_7) = D_x{}^{-1/2} D_y{}^{-1/2} f(x,y)\big|_{x=y=1} = 3.6414$

7) $\overline{SDD}(Li_7) = (S_y D_x + S_x D_y) f(x,y)\big|_{x=y=1} = 22.5$

8) $\overline{H}\,(Li_7) = 2S_x J\, f(x,y)|_{x=y=1} = 3.5381$

9) $\overline{I}\,(Li_7) = S_x J D_x D_y\, f(x,y)\big|_{x=y=1} = 13.662$

10) $\overline{A}\,(Li_7) = S_x{}^3 Q_{-2}\, J D_x{}^3 D_y{}^3\, f(x,y)\big|_{x=y=1} = 95.039$

Table 1: Codescriptors Values for Lithium Clusters Li_n $(n = 4 - 10)$

Li_n	$\overline{M}_1(Li)$	$\overline{M}_2(Li)$	$m\overline{M}_2(Li)$	$\overline{ReZG_3}(Li)$	$\overline{F}(Li)$	$\overline{R}_{-\frac{1}{2}}(Li)$	$\overline{SDD}(Li)$	$\overline{H}(Li)$	$\overline{I}(Li)$	$\overline{A}(Li)$
Li_4	4	4	0.25	16	8	0.5	2	0.5	1	8
Li_5	16	16	1	64	32	2	8	2	4	32
Li_6	24	24	1.5	96	48	3	12	3	6	48
Li_7	58	81	1.3611	490	182	3.6414	22.5	3.5381	13.662	95.039
Li_8	88	120	2.6250	736	272	6.3284	36	6.1667	20.667	149.93
Li_9	130	211	2.1042	1434	442	6.3995	42.33	6.3024	31.681	249.65
Li_{10}	200	476	0.9425	4568	960	4.4389	42.4	4.4278	49.778	571.76

The Binding energy (BE) measures the energy needed to break the cluster into individual Li atoms, indicating the strength of the interactions maintaining the cluster's integrity. To predict the Binding Energy (BE), we performed a curvilinear regression analysis to determine the optimal linear, quadratic, and cubic models. Below (3) is the general form of the regression model, where BE represents binding energy, α_j Represent topological code descriptor coefficients with $j = 1, 2$ & 3 and β Represents the regression model constant.

$$BE = \sum_{j=1}^{3} \alpha_j\, (\text{codescriptor}) + \beta \tag{3}$$

Using SPSS software, we developed the predictive models presented in this section. We then confirmed their reliability by evaluating their F-test values, standard error (SE), and squared correlation coefficients. (R^2). This section analyses three types of regression models: linear, quadratic, and cubic. The analysis focuses on the Binding Energy feature, using (3) and the values provided in Table 1. The data in Tables 2 and 3 reveal the most effective codescriptors for predicting the Binding Energy of Lithium clusters:

- For Linear and Quadratic Models: The Symmetric Division codescriptor $(\overline{SDD})$ Performs best.
- For the Cubic Model: The Randic codescriptor $\left(\overline{R}_{-\frac{1}{2}}\right)$ Stands out as the superior choice.

Table 2: The Coefficient of Determination (R^2) Between the Binding Energy of Lithium Clusters and the Codescriptor, As Calculated by Linear, Quadratic, and Cubic Regression Models

Binding Energy	$\overline{M}_1(Li)$	$\overline{M}_2(Li)$	$m\overline{M}_2(Li)$	$\overline{ReZG_3}(Li)$	$\overline{F}(Li)$	$\overline{R}_{-\frac{1}{2}}(Li)$	$\overline{SDD}(Li)$	$\overline{H}(Li)$	$\overline{I}(Li)$	$\overline{A}(Li)$
Linear	0.68432	0.50579	0.45534	0.39858	0.53445	0.80004	0.86861	0.80476	0.66515	0.50048
Quadratic	0.90248	0.8173	0.56351	0.75462	0.83181	0.92654	0.97426	0.92339	0.89894	0.84197
Cubic	0.9747	0.93192	0.57984	0.88898	0.92464	0.99703	0.98108	0.99314	0.97689	0.97436

$$BE = 0.693 + 0.005\, (\overline{SDD}(Li)) \tag{4}$$

$$BE = 0.63315 + 0.01438\, \big(\overline{SDD}(Li)\big) - 1.94037E - 4\big(\overline{SDD}(Li)\big)^2 \tag{5}$$

$$BE = 0.67284 - 0.04754\left(\overline{R}_{-\frac{1}{2}}(Li)\right) + 0.04594\left(\overline{R}_{-\frac{1}{2}}(Li)\right)^2 - 0.00522\left(\overline{R}_{-1/2}(Li)\right)^3 \quad (6)$$

Table 3: Statistically Validated Models Providing the Most Accurate Estimates for Binding Energy

Regression Model	Curve Equation	d(R^2)	F	SE	SF
Linear	(4)	0.842	33.055	0.038	0.002
Quadratic	(5)	0.961	75.696	0.019	0.001
Cubic	(6)	0.994	335.629	0.007	0.000

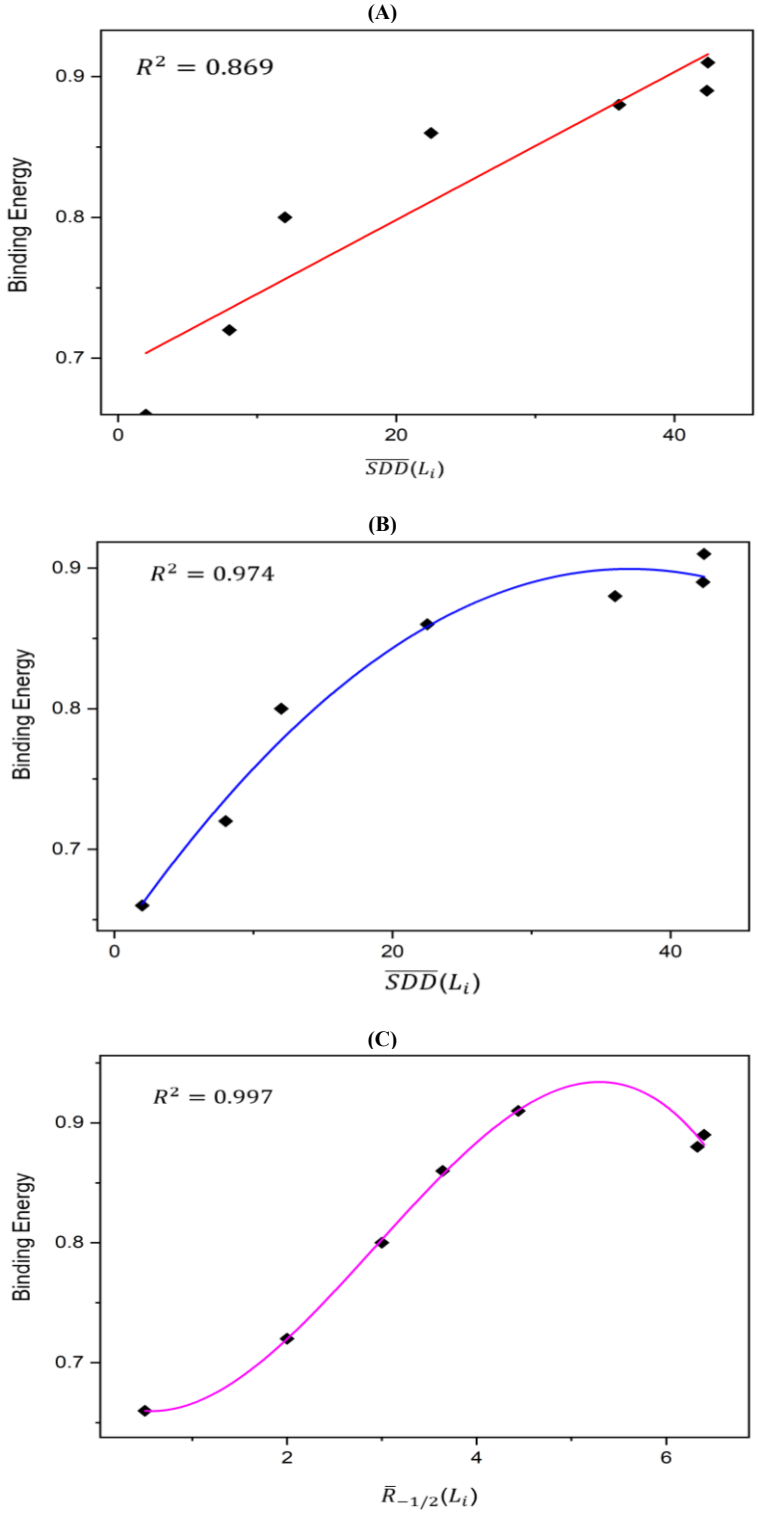

Fig. 3: Regression Plots for the Binding Energy of Lithium Clusters, Showing the Optimal Fits for (A) Linear, (B) Quadratic, and (C) Cubic Models.

A key limitation for predicting the Binding Energy (BE) of any Lithium cluster was that the existing equations (4-6) were only validated for clusters with up to 10 atoms (Table 1). To solve this, we formulated equations (7) and (8) to model the relationship between the codescriptors and the number of Li atoms. These new equations, derived from the best-fitting regression models, allow us to first find the codescriptor values for a cluster of any size. These values are then used in the original equations (4-6) to compute the BE, creating a better applicable predictive tool. Figure 4 illustrates the models from equations (7) and (8).

$$\overline{\mathrm{SDD}} = -29.861(\pm 5.157) + 7.638\ (\pm 0.708)\mathrm{n} \quad (7)$$

$$\overline{\mathrm{R}}_{-\frac{1}{2}} = 19.149(\pm 15.435) - 10.904(\pm 7.215)\mathrm{n} + 1.997(\pm 1.071)\mathrm{n}^2 - 0.105(\pm 0.051)\mathrm{n}^3 \quad (8)$$

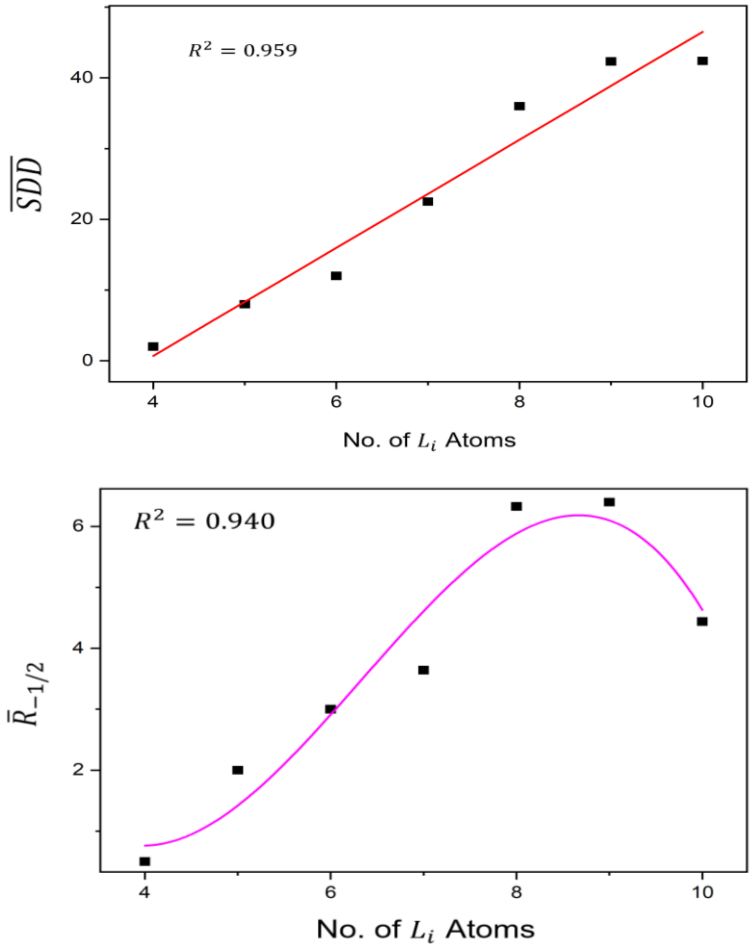

Fig. 4: Regression Plots for the $\overline{\mathrm{SDD}}$ (Linear, Equation 7) and the $\overline{\mathrm{R}}_{-\frac{1}{2}}$ (Cubic, Equation 8) as A Function of the Number of Li Atoms.

3. CoM Polynomial of Hexagonal and Rectangular Porous Nano Graphene Structure

Porous graphene is a material with exceptional capabilities for high-tech applications, created by strategically introducing pores into graphene—a revolutionary, atom-thin sheet of carbon that is extraordinarily strong, light, and conductive. While a perfect sheet of graphene acts as an impenetrable wall, creating these pores unlocks its full potential. A porous framework made from graphene provides a unique combination of benefits that surpasses other porous carbons, effectively forming a nanoscale scaffold that is both strong and highly functional. Due to graphene's inherent mechanical and chemical strength, the resulting material is exceptionally durable and can withstand harsh environments without collapsing. These porous structures feature channels within the sheets and controlled spacing between them, which act as superhighways for the rapid movement of ions and molecules—a critical feature for applications like fast-charging batteries and efficient filtering. Furthermore, the entire framework is electrically conductive, allowing it to transport electrical charges quickly and making it an ideal material for electrodes in energy devices [20-26].

Scientists can design porous graphene in various architectures, such as linear, triangular, rectangular, and hexagonal, to suit specific tasks. Building on previous work, such as the study by Ali et al. [42], which obtained several topological results for linear and triangular structures, our research focuses on a topological analysis of the hexagonal and rectangular porous nanographene structures depicted in Figure 5. Motivated by this wide structural variety, we utilize the CoM Polynomial to develop analytical formulas for key topological codescriptors (TCDs). We then present these TCDs in both tabular and graphical formats, followed by a comparative analysis to reveal trends across the different architectures.

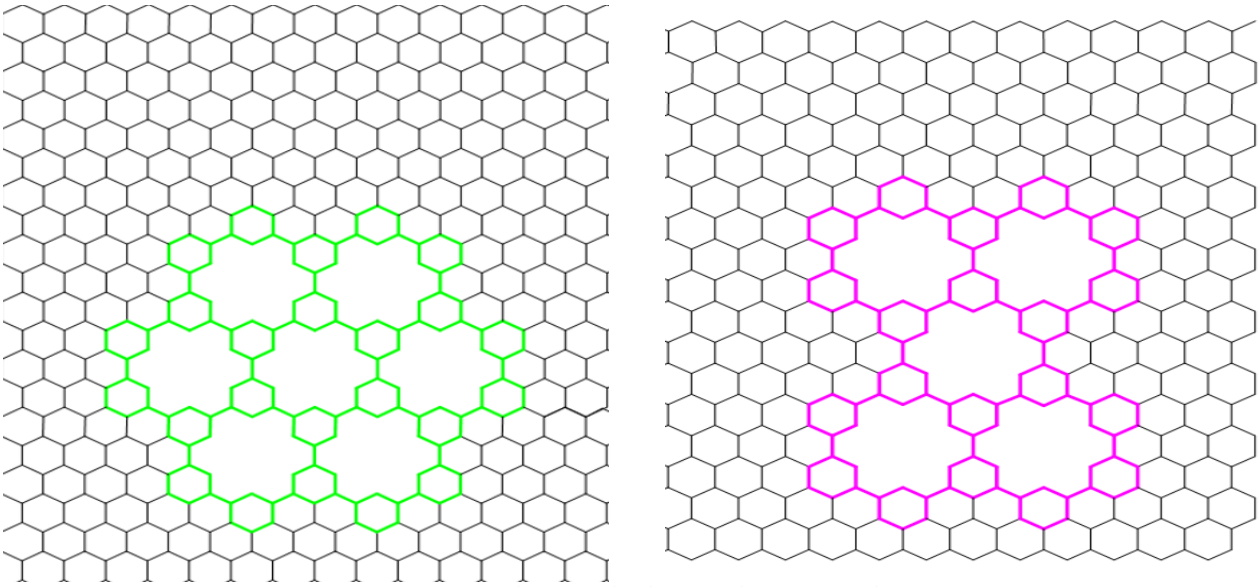

Fig. 5: Structure of Hexagonal and Rectangular Porous Graphene.

3.1. CoM polynomial of hexagonal porous graphene (HPG)

Theorem 1: *The CoM Polynomial for HPG given by*

$CoM(G_{HPG}; x, y) =$

$= (162p^4 + 108p^3 + 9p^2 - 15p)x^2y^2 + (324p^4 - 72p^2 + 12p)x^2y^3 + (162p^4 - 108p^3 + 6p)x^3y^3$

Proof: $|E_{HPG}| = 45p^2 - 3p, |V_{HPG}| = 36p^2$ Is the straightforward deduction from Figure 6. The $|E_{HPG}|$ Classified into three classes according to vertex degrees:

$E_{22} = \{uv \in E_{HPG} | d(u) = 2, d(v) = 2\}$, $E_{23} = \{uv \in E_{HPG} | d(u) = 2, d(v) = 3\}, E_{33} = \{uv \in E_{HPG} | d(u) = 3, d(v) = 3\}$ such that $|E_{22}| = 12p, |E_{23}| = 36p^2 - 12p, |E_{33}| = 9p^2 - 3p$

HPG 's vertex set is classified into two classes according to the degrees.

$n_2 = |V_2| = 18p^2 + 6p$, $n_3 = |V_3| = 18p^2 - 6p$

Using (1), we have

$\bar{m}_{23} = (18p^2 + 6p)(18p^2 - 6p) - (36p^2 - 12p) = 324p^4 - 72p^2 + 12p$

$\bar{m}_{22} = \frac{(18p^2+6p)(18p^2+6p-1)}{2} - 12p$

$= 162p^4 + 108p^3 + 9p^2 - 15p$

Similarly, $\bar{m}_{33} = |\bar{E}_{33}| = = 162p^4 - 108p^3 + 6p$

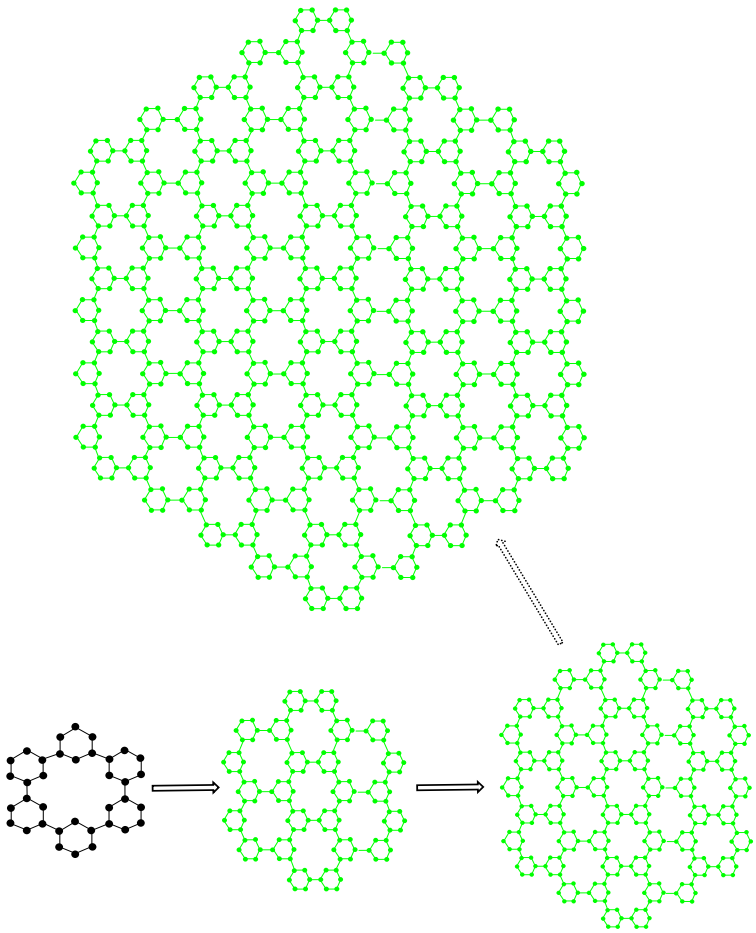

Fig. 6: Molecular Graphs G_{HPG} Of Hexagonal Porous Graphene.

By the definition of CoM Polynomial

$CoM(G_{MG}; x, y) = \sum_{i\le j} \bar{m}_{ij}(G_{MG})x^i y^j$

$CoM(G_{HPG}; x, y) = \sum_{2\le 2} \bar{m}_{22}\, x^2y^2 + \sum_{2\le 3} \bar{m}_{23}\, x^2y^3 + \sum_{3\le 3} \bar{m}_{33}\, x^3y^3$

$= |\bar{E}_{22}|x^2y^2 + |\bar{E}_{23}|x^2y^3 + |\bar{E}_{33}|\, x^3y^3$

$= (162p^4 + 108p^3 + 9p^2 - 15p)x^2y^2 + (324p^4 - 72p^2 + 12p)x^2y^3 + (162p^4 - 108p^3 + 6p)x^3y^3$

Hence the result.

Proposition 1: The topological codescriptors for HPG are given by

1) $\bar{M}_1(G_{HPG}) = (D_x + D_y)f(x,y)\big|_{x=y=1} = 3240p^4 - 216p^3 - 324p^2 + 36p.$

2) $\bar{M}_2(G_{HPG}) = D_xD_yf(x,y)\big|_{x=y=1} = 4050p^4 - 540p^3 - 396p^2 + 66p.$

3) $m\bar{M}_2(G_{HPG}) = S_xS_yf(x,y)\big|_{x=y=1} = \frac{225}{2}p^4 + 15p^3 - \frac{39}{4}p^2 - \frac{13}{12}p$

4) $\overline{ReZG_3}(G_{HPG}) = D_xD_y(D_x + D_y)f(x,y)\big|_{x=y=1} = 21060p^4 - 4104p^3 - 2016p^2 + 444p.$

5) $\bar{F}(G_{HPG}) = (D_x^2 + D_y^2)(f(x,y))\big|_{x=y=1} = 8424p^4 - 1080p^3 - 864p^2 + 144p.$

6) $\bar{R}_k(G_{HPG}) = D_x{}^kD_y{}^kf(x,y)\big|_{x=y=1} = 2^{2k}(162p^4 + 108p^3 + 9p^2 - 15p) + 2^k3^k(324p^4 - 72p^2 + 12p) + 3^{2k}(162p^4 - 108p^3 + 6p)$.

7) $\overline{R\bar{R}}_k(G_{HPG}) = S_x{}^kS_y{}^kf(x,y)\big|_{x=y=1} = (162p^4 + 108p^3 + 9p^2 - 15p)\frac{1}{(2)^{2k}} + (324p^4 - 72p^2 + 12p)\frac{1}{(2)^k(3)^k} + (162p^4 - 108p^3 + 6p)\frac{1}{(3)^{2k}}.$

8) $\overline{SDD}(G_{HPG}) = (S_yD_x + S_xD_y)f(x,y)\big|_{x=y=1} = 1350p^4 - 138p^2 + 8p$

9) $\overline{H}\,(G_{HPG}) = 2S_xJ\,f(x,y)|_{x=y=1} = \frac{1323}{5}p^4 + 18p^3 - \frac{243}{10}p^2 - \frac{7}{10}p$

10) $\overline{I}\,(G_{HPG}) = S_xJD_xD_y\,f(x,y)\big|_{x=y=1} = \frac{3969}{5}p^4 - 54p^3 - \frac{387}{5}p^2 + \frac{42}{5}p$

11) $\overline{A}\,(G_{HPG}) = S_x{}^3Q_{-2}\,JD_x{}^3D_y{}^3\,f(x,y)\big|_{x=y=1} = \frac{183465}{32}p^4 - \frac{5859}{16}p^3 - 504p^2 + \frac{1419}{32}p.$

Proof: Let
$f(x,y) = CoM(G_{HPG};x,y) = (162p^4 + 108p^3 + 9p^2 - 15p)x^2y^2 + (324p^4 - 72p^2 + 12p)x^2y^3 + (162p^4 - 108p^3 + 6p)x^3y^3$,
then

- $D_xf(x,y) = 2(162p^4 + 108p^3 + 9p^2 - 15p)x^2y^2 + 2(324p^4 - 72p^2 + 12p)x^2y^3 + 3(162p^4 - 108p^3 + 6p)x^3y^3.$
- $D_yf(x,y) = 2(162p^4 + 108p^3 + 9p^2 - 15p)x^2y^2 + 3(324p^4 - 72p^2 + 12p)x^2y^3 + 3(162p^4 - 108p^3 + 6p)x^3y^3.$
- $(D_x + D_y)(f(x,y)) = 4(162p^4 + 108p^3 + 9p^2 - 15p)x^2y^2 + 5(324p^4 - 72p^2 + 12p)x^2y^3 + 6(162p^4 - 108p^3 + 6p)x^3y^3.$
- $D_yD_x\big(f(x,y)\big) = 4(162p^4 + 108p^3 + 9p^2 - 15p)x^2y^2 + 6(324p^4 - 72p^2 + 12p)x^2y^3 + 9(162p^4 - 108p^3 + 6p)x^3y^3.$
- $\big(D_x^2 + D_y^2\big)\big(f(x,y)\big) = 8(162p^4 + 108p^3 + 9p^2 - 15p)x^2y^2 + 13(324p^4 - 72p^2 + 12p)x^2y^3 + 18(162p^4 - 108p^3 + 6p)x^3y^3.$
- $D_x{}^kD_y{}^k\big(f(x,y)\big) = 2^{2k}(162p^4 + 108p^3 + 9p^2 - 15p)x^2y^2 + 2^k3^k(324p^4 - 72p^2 + 12p)x^2y^3 + 3^{2k}(162p^4 - 108p^3 + 6p)x^3y^3.$
- $D_xD_y(D_x + D_y)(f(x,y) = 16(162p^4 + 108p^3 + 9p^2 - 15p)x^2y^2 + 30(324p^4 - 72p^2 + 12p)x^2y^3 + 54(162p^4 - 108p^3 + 6p)x^3y^3.$
- $S_xS_y\big(f(x,y)\big) = (162p^4 + 108p^3 + 9p^2 - 15p)\frac{1}{(2)(2)}x^2y^2 + (324p^4 - 72p^2 + 12p)\frac{1}{(2)(3)}x^2y^3 + (162p^4 - 108p^3 + 6p)\frac{1}{(3)(3)}x^3y^3.$
- $S_x{}^kS_y{}^k(f(x,y)) = (162p^4 + 108p^3 + 9p^2 - 15p)\frac{1}{(2)^{2k}}x^2y^2 + (324p^4 - 72p^2 + 12p)\frac{1}{(2)^k(3)^k}x^2y^3 + (162p^4 - 108p^3 + 6p)\frac{1}{(3)^{2k}}x^3y^3.$
- $(S_yD_x + S_xD_y)(f(x,y)) = 2(162p^4 + 108p^3 + 9p^2 - 15p)x^2y^2 + \frac{13}{6}(324p^4 - 72p^2 + 12p)x^2y^3 + 2(162p^4 - 108p^3 + 6p)x^3y^3.$
- $S_x\,J\,\big(f(x,y)\big) = (162p^4 + 108p^3 + 9p^2 - 15p)\frac{1}{4}x^4 + (324p^4 - 72p^2 + 12p)\frac{1}{5}x^5 + (162p^4 - 108p^3 + 6p)\frac{1}{6}x^6.$
- $S_x\,J\,D_yD_x(f(x,y)) = (162p^4 + 108p^3 + 9p^2 - 15p)x^4 + (324p^4 - 72p^2 + 12p)\left(\frac{6}{5}\right)x^5 + (162p^4 - 108p^3 + 6p)\left(\frac{3}{2}\right)x^6.$
- $S_x{}^3Q_{-2}\,J\,D_x{}^3D_y{}^3\big(f(x,y)\big) = 8(162p^4 + 108p^3 + 9p^2 - 15p)x^2 + 8(324p^4 - 72p^2 + 12p)x^3 + \frac{729}{64}(162p^4 - 108p^3 + 6p)x^4.$

1) $\overline{M}_1(G_{HPG}) = \big(D_x + D_y\big)f(x,y)\big|_{x=y=1} = 3240p^4 - 216p^3 - 324p^2 + 36p.$

2) $\overline{M}_2(G_{HPG}) = D_xD_yf(x,y)\big|_{x=y=1} = 4050p^4 - 540p^3 - 396p^2 + 66p.$

3) $m\overline{M}_2(G_{HPG}) = S_xS_yf(x,y)\big|_{x=y=1} = \frac{225}{2}p^4 + 15p^3 - \frac{39}{4}p^2 - \frac{13}{12}p$

4) $\overline{ReZG_3}(G_{HPG}) = D_xD_y(D_x + D_y)f(x,y)\big|_{x=y=1} = 21060p^4 - 4104p^3 - 2016p^2 + 444p.$

5) $\overline{F}(G_{HPG}) = (D_x^2 + D_y^2)(f(x,y))\big|_{x=y=1} = 8424p^4 - 1080p^3 - 864p^2 + 144p.$

6) $\overline{R}_k(G_{HPG}) = D_x{}^kD_y{}^kf(x,y)\big|_{x=y=1} = 2^{2k}(162p^4 + 108p^3 + 9p^2 - 15p) + 2^k3^k(324p^4 - 72p^2 + 12p) + 3^{2k}(162p^4 - 108p^3 + 6p)$.

7) $\overline{RR}_k(G_{HPG}) = S_x{}^kS_y{}^kf(x,y)\big|_{x=y=1} = (162p^4 + 108p^3 + 9p^2 - 15p)\frac{1}{(2)^{2k}} + (324p^4 - 72p^2 + 12p)\frac{1}{(2)^k(3)^k} + (162p^4 - 108p^3 + 6p)\frac{1}{(3)^{2k}}.$

8) $\overline{SDD}(G_{HPG}) = (S_yD_x + S_xD_y)f(x,y)\big|_{x=y=1} = 1350p^4 - 138p^2 + 8p$

9) $\overline{H}(G_{HPG}) = 2S_xJ\, f(x,y)|_{x=y=1} = \frac{1323}{5}p^4 + 18p^3 - \frac{243}{10}p^2 - \frac{7}{10}p$

10) $\overline{I}(G_{HPG}) = S_xJD_xD_y\, f(x,y)\big|_{x=y=1} = \frac{3969}{5}p^4 - 54p^3 - \frac{387}{5}p^2 + \frac{42}{5}p$

11) $\overline{A}(G_{HPG}) = S_x{}^3Q_{-2}\, JD_x{}^3D_y{}^3\, f(x,y)\big|_{x=y=1} = \frac{183465}{32}p^4 - \frac{5859}{16}p^3 - 504p^2 + \frac{1419}{32}p.$

Table 4: Numerical Values of TCDs of HPG for $p = 1 - 10$.

(p)	$\overline{M}_1(G_{HPG})$	$\overline{M}_2(G_{HPG})$	$m\overline{M}_2(G_{HPG})$	$\overline{ReZG}_3(G_{HPG})$	$\overline{F}(G_{HPG})$	$\overline{R}_{-\frac{1}{2}}(G_{HPG})$	$\overline{SDD}(G_{HPG})$	$\overline{H}(G_{HPG})$	$\overline{I}(G_{HPG})$	$\overline{A}(G_{HPG})$
(1)	2736	3180	116.67	15384	6624	259.78	1220	257.60	670.8	4907.44
(2)	48888	59028	1878.83	296952	122976	4319.6	21064	4279.0	11976.0	86875.69
(3)	253800	310104	9426.50	1578240	645840	21909.22	108132	21697.8	62168.4	450105.75
(4)	810576	996168	29599.67	5098224	2074176	69173.04	343424	68498.0	198552.0	1436397.38
(5)	1990080	2454180	71938.33	12601320	5109120	168669.92	840340	167014.0	487482.0	3525149.06
(6)	4140936	5118300	148682.5	26337384	10653984	349373.31	1744680	345930.6	1014364.8	7333358.06
(7)	7689528	9519888	274772.17	49061712	19814256	646671.14	3234644	640283.0	1883658.0	13615620.38
(8)	13140000	16287504	467847.33	84035040	33897600	1102365.92	5520832	1091456.8	3218870.40	23264130.75
(9)	21074256	26146908	748248	135023544	54413856	1764674.71	8846244	1747188.0	5162562	37308682.69
(10)	32151960	39921060	1139014.17	206298840	83075040	2688229.1	13486280	2661563.0	7876344	56916668.44

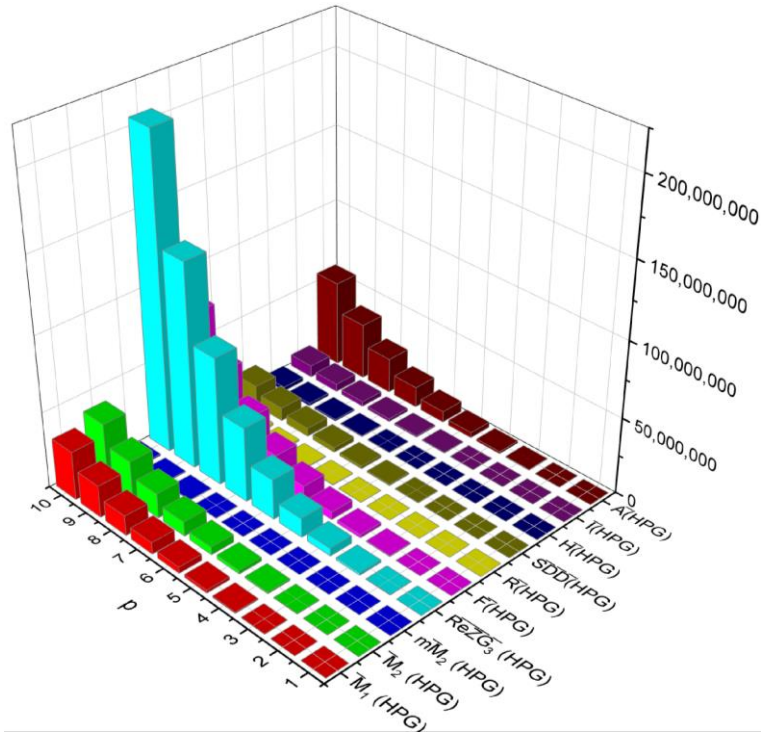

Fig. 7: Graphical Visualization of Table 4.

3.2. CoM polynomial of rectangular porous graphene (RPG)

Theorem 2: *The CoM Polynomial for RPG given by*

$CoM(G_{RPG}; x, y) =$

$= (72p^2q^2 + 120pq^2 + 24p^2q + 14pq + 50q^2 + 2p^2 - 13q - 5p)x^2y^2 + (144p^2q^2 + 144pq^2 - 40pq + 20q^2 - 4p^2 - 4q + 4p)x^2y^3 + (72p^2q^2 + 24pq^2 - 24p^2q - 16pq + 2q^2 + 2p^2 - 2q + 2p)x^3y^3$

Proof: From the Figure-8, it is straightforward to deduce that $|E_{RPG}| = 30pq + 13q - p, |V_{RPG}| = 24pq + 12q$. The $|E_{RPG}|$ Can be classified into three classes based on the vertex degrees:

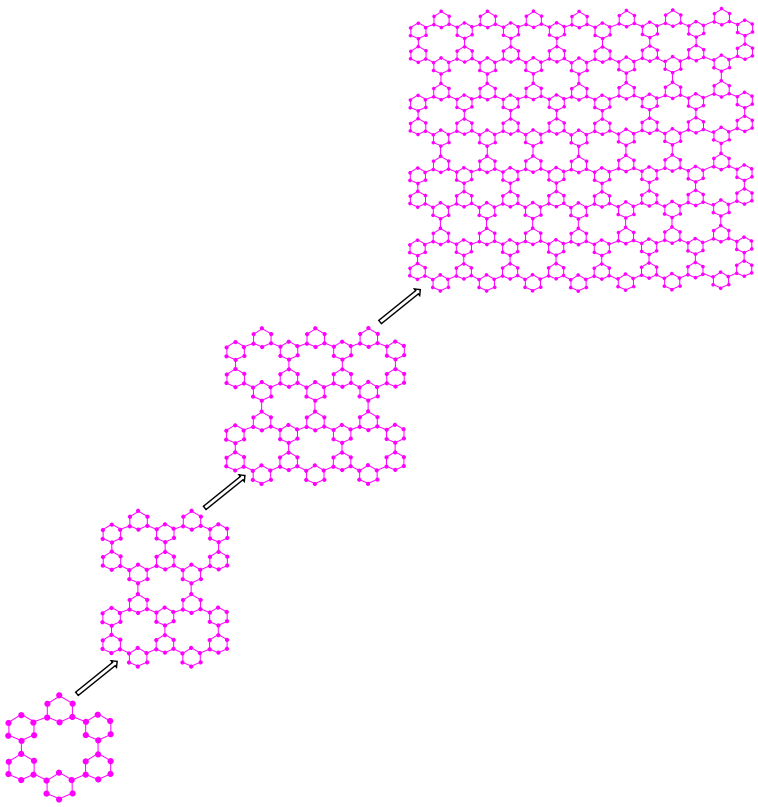

Fig. 8: Molecular Graphs G_{RPG} Of Rectangular Porous Graphene.

$E_{22} = \{uv \in E_{RPG} | d(u) = 2, d(v) = 2\}$, $E_{23} = \{uv \in E_{RPG} | d(u) = 2, d(v) = 3\}, E_{33} = \{uv \in E_{RPG} | d(u) = 3, d(v) = 3\}$

such that $|E_{22}| = 4p + 8q, |E_{23}| = 24pq + 4q - 4p, |E_{33}| = 6pq + q - p.$

Similarly, RPG 's vertex set can be classified into two classes based on their degrees. $n_2 = |V_2| = 12pq + 10q + 2p$, $n_3 = |V_3| = 12pq + 2q - 2p$

Using 2, we have $\bar{m}_{23} = (12pq + 10q + 2p)(12pq + 2q - 2p) - (24pq + 4q - 4p)$

$= 144p^2q^2 + 144pq^2 - 40pq + 20q^2 - 4p^2 - 4q + 4p$

$$\bar{m}_{22} = \frac{(12pq + 10q + 2p)(12pq + 10q + 2p - 1)}{2} - (4p + 8q)$$

$= 72p^2q^2 + 120pq^2 + 24p^2q + 14pq + 50q^2 + 2p^2 - 13q - 5p$

Similarly, $\bar{m}_{33} = |\bar{E}_{33}| = 72p^2q^2 + 24pq^2 - 24p^2q - 16pq + 2q^2 + 2p^2 - 2q + 2p$

By the definition of CoM Polynomial

$CoM(G_{MG}; x, y) = \sum_{i \le j} \bar{m}_{ij}(G_{MG}) x^i y^j$

$CoM(G_{RPG}; x, y) = \sum_{2 \le 2} \bar{m}_{22}\, x^2y^2 + \sum_{2 \le 3} \bar{m}_{23}\, x^2y^3 + \sum_{3 \le 3} \bar{m}_{33}\, x^3y^3$

$= |\bar{E}_{22}| x^2y^2 + |\bar{E}_{23}| x^2y^3 + |\bar{E}_{33}|\, x^3y^3$

$= (72p^2q^2 + 120pq^2 + 24p^2q + 14pq + 50q^2 + 2p^2 - 13q - 5p)x^2y^2 + (144p^2q^2 + 144pq^2 - 40pq + 20q^2 - 4p^2 - 4q + 4p)x^2y^3 + (72p^2q^2 + 24pq^2 - 24p^2q - 16pq + 2q^2 + 2p^2 - 2q + 2p\ )x^3y^3$

Hence the result.
Proposition 2: The topological codescriptors for RPG are given by

1) $\bar{M}_1(G_{RPG}) = 1440p^2q^2 - 48p^2q + 1344pq^2 + 312q^2 + 12p - 240pq - 84q.$

2) $\bar{M}_2(G_{RPG}) = 1800p^2q^2 - 120p^2q + 2p^2 + 1560pq^2 + 338q^2 + 22p - 328pq - 94q.$

3) $m\bar{M}_2(G_{RPG}) = 50p^2q^2 + \frac{10}{3}p^2q + \frac{1}{18}p^2 + \frac{170}{3}pq^2 + \frac{289}{18}q^2 - \frac{13}{36}p - \frac{89}{18}pq - \frac{149}{36}q$

4) $\overline{ReZG_3}(G_{RPG}) = 9360p^2q^2 - 912p^2q + 20p^2 + 7536pq^2 + 1508q^2 + 148p - 1840pq - 436q.$

5) $\overline{F}(G_{RPG}) = 3744p^2q^2 - 240p^2q + 3264pq^2 + 696q^2 + 48p - 696pq - 192q.$

6) $\overline{R}_k(G_{RPG}) = 2^{2k}(72p^2q^2 + 120pq^2 + 24p^2q + 14pq + 50q^2 + 2p^2 - 13q - 5p) + 2^k3^k(144p^2q^2 + 144pq^2 - 40pq + 20q^2 - 4p^2 - 4q + 4p) + 3^{2k}(72p^2q^2 + 24pq^2 - 24p^2q - 16pq + 2q^2 + 2p^2 - 2q + 2p).$

7) $\overline{R\overline{R}}_k(G_{RPG}) = (72p^2q^2 + 120pq^2 + 24p^2q + 14pq + 50q^2 + 2p^2 - 13q - 5p)\frac{1}{(2)^{2k}} + (144p^2q^2 + 144pq^2 - 40pq + 20q^2 - 4p^2 - 4q + 4p)\frac{1}{(2)^k(3)^k} + (72p^2q^2 + 24pq^2 - 24p^2q - 16pq + 2q^2 + 2p^2 - 2q + 2p)\frac{1}{(3)^{2k}}.$

8) $\overline{SDD}(G_{RPG}) = 600p^2q^2 - \frac{2}{3}p^2 + 600pq^2 + \frac{442}{3}q^2 + \frac{8}{3}p - \frac{272}{3}pq - \frac{116}{3}q.$

9) $\overline{H}(G_{RPG}) = \frac{294}{5}p^2q^2 + 2p^2q + \frac{1}{30}p^2 + \frac{314}{5}pq^2 + \frac{101}{6}q^2 - \frac{7}{60}p - \frac{43}{6}pq - \frac{263}{60}q.$

10) $\overline{I}(G_{RPG}) = \frac{1764}{5}p^2q^2 - 12p^2q + \frac{1}{5}p^2 + \frac{1644}{5}pq^2 + 77q^2 + \frac{14}{5}p - 58pq - \frac{104}{5}q.$

11) $\overline{A}(G_{RPG}) = \frac{20385}{8}p^2q^2 - \frac{651}{8}p^2q + \frac{217}{32}p^2 + \frac{19083}{8}pq^2 + \frac{18649}{32}q^2 + \frac{473}{32}p - \frac{1561}{4}pq - \frac{5081}{32}q.$

Proof: Let

$f(x,y) = CoM(G_{RPG}; x, y) = (72p^2q^2 + 120pq^2 + 24p^2q + 14pq + 50q^2 + 2p^2 - 13q - 5p)x^2y^2 + (144p^2q^2 + 144pq^2 - 40pq + 20q^2 - 4p^2 - 4q + 4p)x^2y^3 + (72p^2q^2 + 24pq^2 - 24p^2q - 16pq + 2q^2 + 2p^2 - 2q + 2p)x^3y^3,$

then

- $D_xf(x,y) = 2(72p^2q^2 + 120pq^2 + 24p^2q + 14pq + 50q^2 + 2p^2 - 13q - 5p)x^2y^2 + 2(144p^2q^2 + 144pq^2 - 40pq + 20q^2 - 4p^2 - 4q + 4p)x^2y^3 + 3(72p^2q^2 + 24pq^2 - 24p^2q - 16pq + 2q^2 + 2p^2 - 2q + 2p)x^3y^3.$
- $D_yf(x,y) = 2(72p^2q^2 + 120pq^2 + 24p^2q + 14pq + 50q^2 + 2p^2 - 13q - 5p)x^2y^2 + 3(144p^2q^2 + 144pq^2 - 40pq + 20q^2 - 4p^2 - 4q + 4p)x^2y^3 + 3(72p^2q^2 + 24pq^2 - 24p^2q - 16pq + 2q^2 + 2p^2 - 2q + 2p)x^3y^3.$
- $(D_x + D_y)(f(x,y)) = 4(72p^2q^2 + 120pq^2 + 24p^2q + 14pq + 50q^2 + 2p^2 - 13q - 5p)x^2y^2 + 5(144p^2q^2 + 144pq^2 - 40pq + 20q^2 - 4p^2 - 4q + 4p)x^2y^3 + 6(72p^2q^2 + 24pq^2 - 24p^2q - 16pq + 2q^2 + 2p^2 - 2q + 2p)x^3y^3.$
- $D_yD_x(f(x,y)) = 4(72p^2q^2 + 120pq^2 + 24p^2q + 14pq + 50q^2 + 2p^2 - 13q - 5p)x^2y^2 + 6(144p^2q^2 + 144pq^2 - 40pq + 20q^2 - 4p^2 - 4q + 4p)x^2y^3 + 9(72p^2q^2 + 24pq^2 - 24p^2q - 16pq + 2q^2 + 2p^2 - 2q + 2p)x^3y^3.$
- $(D_x^2 + D_y^2)(f(x,y)) = 8(72p^2q^2 + 120pq^2 + 24p^2q + 14pq + 50q^2 + 2p^2 - 13q - 5p)x^2y^2 + 13(144p^2q^2 + 144pq^2 - 40pq + 20q^2 - 4p^2 - 4q + 4p)x^2y^3 + 18(72p^2q^2 + 24pq^2 - 24p^2q - 16pq + 2q^2 + 2p^2 - 2q + 2p)x^3y^3.$
- $D_x^kD_y^k(f(x,y)) = 2^{2k}(72p^2q^2 + 120pq^2 + 24p^2q + 14pq + 50q^2 + 2p^2 - 13q - 5p)x^2y^2 + 2^k3^k(144p^2q^2 + 144pq^2 - 40pq + 20q^2 - 4p^2 - 4q + 4p)x^2y^3 + 3^{2k}(72p^2q^2 + 24pq^2 - 24p^2q - 16pq + 2q^2 + 2p^2 - 2q + 2p)x^3y^3.$
- $D_xD_y(D_x + D_y)(f(x,y) = 16(72p^2q^2 + 120pq^2 + 24p^2q + 14pq + 50q^2 + 2p^2 - 13q - 5p)x^2y^2 + 30(144p^2q^2 + 144pq^2 - 40pq + 20q^2 - 4p^2 - 4q + 4p)x^2y^3 + 54(72p^2q^2 + 24pq^2 - 24p^2q - 16pq + 2q^2 + 2p^2 - 2q + 2p)x^3y^3.$
- $S_xS_y(f(x,y)) = (72p^2q^2 + 120pq^2 + 24p^2q + 14pq + 50q^2 + 2p^2 - 13q - 5p)\frac{1}{(2)(2)}x^2y^2 + (144p^2q^2 + 144pq^2 - 40pq + 20q^2 - 4p^2 - 4q + 4p)\frac{1}{(2)(3)}x^2y^3 + (72p^2q^2 + 24pq^2 - 24p^2q - 16pq + 2q^2 + 2p^2 - 2q + 2p)\frac{1}{(3)(3)}x^3y^3.$
- $S_x^kS_y^k(f(x,y)) = (72p^2q^2 + 120pq^2 + 24p^2q + 14pq + 50q^2 + 2p^2 - 13q - 5p)\frac{1}{(2)^{2k}}x^2y^2 + (144p^2q^2 + 144pq^2 - 40pq + 20q^2 - 4p^2 - 4q + 4p)\frac{1}{(2)^k(3)^k}x^2y^3 + (72p^2q^2 + 24pq^2 - 24p^2q - 16pq + 2q^2 + 2p^2 - 2q + 2p)\frac{1}{(3)^{2k}}x^3y^3.$
- $(S_yD_x + S_xD_y)(f(x,y)) = 2(72p^2q^2 + 120pq^2 + 24p^2q + 14pq + 50q^2 + 2p^2 - 13q - 5p)x^2y^2 + \frac{13}{6}(144p^2q^2 + 144pq^2 - 40pq + 20q^2 - 4p^2 - 4q + 4p)x^2y^3 + 2(72p^2q^2 + 24pq^2 - 24p^2q - 16pq + 2q^2 + 2p^2 - 2q + 2p)x^3y^3.$
- $S_x\,J\,(f(x,y)) = (72p^2q^2 + 120pq^2 + 24p^2q + 14pq + 50q^2 + 2p^2 - 13q - 5p)\frac{1}{4}x^4 + (144p^2q^2 + 144pq^2 - 40pq + 20q^2 - 4p^2 - 4q + 4p)\frac{1}{5}x^5 + (72p^2q^2 + 24pq^2 - 24p^2q - 16pq + 2q^2 + 2p^2 - 2q + 2p)\frac{1}{6}x^6.$
- $S_x\,J\,D_yD_x(f(x,y)) = (72p^2q^2 + 120pq^2 + 24p^2q + 14pq + 50q^2 + 2p^2 - 13q - 5p)x^4 + (144p^2q^2 + 144pq^2 - 40pq + 20q^2 - 4p^2 - 4q + 4p)\left(\frac{6}{5}\right)x^5 + (72p^2q^2 + 24pq^2 - 24p^2q - 16pq + 2q^2 + 2p^2 - 2q + 2p)\left(\frac{3}{2}\right)x^6.$
- $S_x^3Q_{-2}\,J\,D_x^3D_y^3(f(x,y)) = 8(72p^2q^2 + 120pq^2 + 24p^2q + 14pq + 50q^2 + 2p^2 - 13q - 5p)x^2 + 8(144p^2q^2 + 144pq^2 - 40pq + 20q^2 - 4p^2 - 4q + 4p)x^3 + \frac{729}{64}(72p^2q^2 + 24pq^2 - 24p^2q - 16pq + 2q^2 + 2p^2 - 2q + 2p)x^4.$

1) $\bar{M}_1(G_{RPG}) = (D_x + D_y)f(x,y)\big|_{x=y=1} = 1440p^2q^2 - 48p^2q + 1344pq^2 + 312q^2 + 12p - 240pq - 84q.$

2) $\bar{M}_2(G_{RPG}) = D_xD_yf(x,y)\big|_{x=y=1} = 1800p^2q^2 - 120p^2q + 2p^2 + 1560pq^2 + 338q^2 + 22p - 328pq - 94q.$

3) $m\bar{M}_2(G_{RPG}) = S_xS_yf(x,y)\big|_{x=y=1} = 50p^2q^2 + \frac{10}{3}p^2q + \frac{1}{18}p^2 + \frac{170}{3}pq^2 + \frac{289}{18}q^2 - \frac{13}{36}p - \frac{89}{18}pq - \frac{149}{36}q$

4) $\overline{ReZG_3}(G_{RPG}) = D_xD_y(D_x + D_y)f(x,y)\big|_{x=y=1} = 9360p^2q^2 - 912p^2q + 20p^2 + 7536pq^2 + 1508q^2 + 148p - 1840pq - 436q$

5) $\bar{F}(G_{RPG}) = (D_x^2 + D_y^2)(f(x,y))\big|_{x=y=1} = 3744p^2q^2 - 240p^2q + 3264pq^2 + 696q^2 + 48p - 696pq - 192q.$

6) $\bar{R}_k(G_{RPG}) = D_x{}^kD_y{}^kf(x,y)\big|_{x=y=1} = 2^{2k}(72p^2q^2 + 120pq^2 + 24p^2q + 14pq + 50q^2 + 2p^2 - 13q - 5p) + 2^k3^k(144p^2q^2 + 144pq^2 - 40pq + 20q^2 - 4p^2 - 4q + 4p) + 3^{2k}(72p^2q^2 + 24pq^2 - 24p^2q - 16pq + 2q^2 + 2p^2 - 2q + 2p)$.

7) $\overline{RR}_k(G_{RPG}) = S_x{}^kS_y{}^kf(x,y)\big|_{x=y=1} = (72p^2q^2 + 120pq^2 + 24p^2q + 14pq + 50q^2 + 2p^2 - 13q - 5p)\frac{1}{(2)^{2k}} + (144p^2q^2 + 144pq^2 - 40pq + 20q^2 - 4p^2 - 4q + 4p)\frac{1}{(2)^k(3)^k} + (72p^2q^2 + 24pq^2 - 24p^2q - 16pq + 2q^2 + 2p^2 - 2q + 2p)\frac{1}{(3)^{2k}}.$

8) $\overline{SDD}(G_{RPG}) = (S_yD_x + S_xD_y)f(x,y)\big|_{x=y=1} = 600p^2q^2 - \frac{2}{3}p^2 + 600pq^2 + \frac{442}{3}q^2 + \frac{8}{3}p - \frac{272}{3}pq - \frac{116}{3}q$

9) $\bar{H}(G_{RPG}) = 2S_xJ\,f(x,y)|_{x=y=1} = \frac{294}{5}p^2q^2 + 2p^2q + \frac{1}{30}p^2 + \frac{314}{5}pq^2 + \frac{101}{6}q^2 - \frac{7}{60}p - \frac{43}{6}pq - \frac{263}{60}q$

10) $\bar{I}(G_{RPG}) = S_xJD_xD_y\,f(x,y)\big|_{x=y=1} = \frac{1764}{5}p^2q^2 - 12p^2q + \frac{1}{5}p^2 + \frac{1644}{5}pq^2 + 77q^2 + \frac{14}{5}p - 58pq - \frac{104}{5}q$

11) $\bar{A}(G_{RPG}) = S_x{}^3Q_{-2}\,JD_x{}^3D_y{}^3\,f(x,y)\big|_{x=y=1} = \frac{20385}{8}p^2q^2 - \frac{651}{8}p^2q + \frac{217}{32}p^2 + \frac{19083}{8}pq^2 + \frac{18649}{32}q^2 + \frac{473}{32}p - \frac{1561}{4}pq - \frac{5081}{32}q$.

Table 5: Numerical Values of TCDs of RPG for $p, q = 1 - 10$

(p,q)	$\bar{M}_1(G_{RPG})$	$\bar{M}_2(G_{RPG})$	$m\bar{M}_2(G_{RPG})$	$\overline{ReZG_3}(G_{RPG})$	$\bar{F}(G_{RPG})$	$\bar{R}_{-\frac{1}{2}}(G_{RPG})$	$\overline{SDD}(G_{RPG})$	$\bar{H}(G_{RPG})$	$\bar{I}(G_{RPG})$	$\bar{A}(G_{RPG})$
(1,1)	2736	3180	116.67	15384	6624	259.78	1220	257.60	670.8	4907.4
(2,2)	33552	40224	1315.67	200928	83808	3005.7	14552	2978.0	8220.0	59711.2
(3,3)	152064	184572	5757.0	933336	384480	13299.0	65196	13172.4	37249.2	269967.9
(4,4)	452448	552864	16800.67	2813952	1151424	39051.0	192752	38674.4	110827.2	802389.0
(5,5)	1063440	1304940	39006.67	6668760	2717280	91026.0	451220	90140.0	260490.0	1884840.9
(6,6)	2148336	2643840	78135.0	13548384	5504544	182840.0	909000	181047.6	526240.8	3806345.2
(7,7)	3904992	4815804	141145.6	24728088	10025568	330940.0	1648892	327698.0	956550.0	6917078.4
(8,8)	6565824	8110272	236198.6	41707776	16882560	554690.0	2768096	549214.4	1608355.2	11628372.0
(9,9)	10397808	12859884	372654.0	66211992	26767584	876200.0	4378212	867542.4	2547061.2	18412712.4
(10,10)	15702480	19440480	561071.6	100189920	40462560	1320495.0	6605240	1307450.0	3846540.0	27803741.2

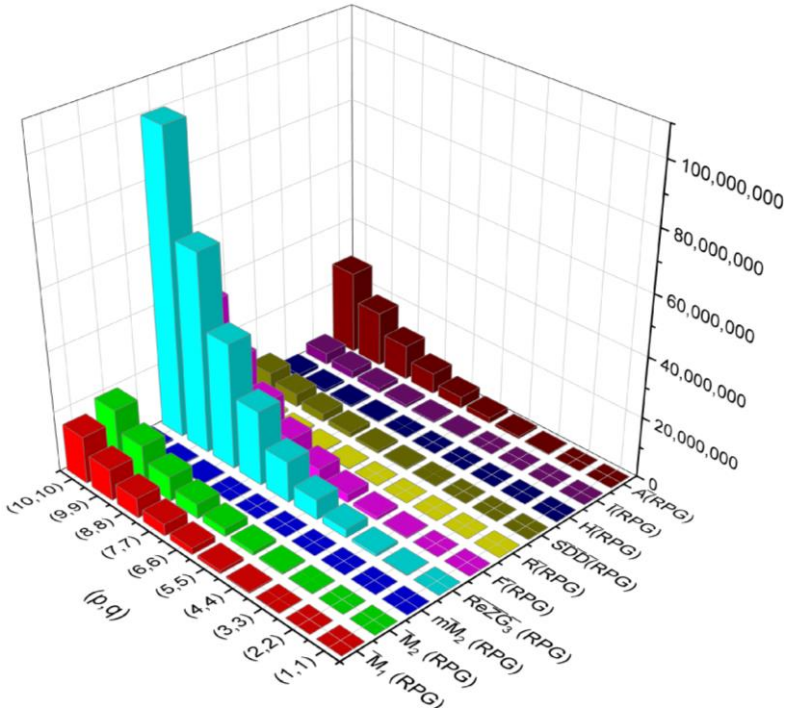

Fig. 9: Graphical Visualization of Table 5.

3.3. Comparative analysis: hexagonal (HPG) vs. rectangular porous graphene (RPG)

In this subsection, the numerical data reported in Tables 4 and 5 (HPG and RPG, respectively) are interpreted with the intent of linking topological growth behaviour to plausible physicochemical consequences. Such comparative interpretation substantially strengthens the analytical findings, because it provides a theoretical rationale for why one porous topology may be more favourable than the other in materials selection for electrochemical devices. A direct comparison of these values reveals significant and consistent differences between the two structures, which can be interpreted to suggest variations in their physicochemical properties. To facilitate a direct comparison, let's look at the $\overline{M}_1$, a TCD related to molecular surface area and branching, and the $\overline{A}$, which is related to the overall size and complexity of the structure. The TCD values are nearly identical for the smallest structure. ($p = 1$) For HPG and RPG. This suggests that the initial unit cell structural differences are negligible in this case. As the size parameter increases, the values for HPG consistently exceed the corresponding values for RPG. For example, at $p = q = 10$, $\overline{M}_1(\text{HPG}) = 32{,}151{,}960$ It is approximately twice the value for $\overline{M}_1(\text{RPG}) = 15{,}702{,}480$. This trend holds across all listed TCDs, ($\overline{M}_1, \overline{M}_2, \overline{mM}_2, \overline{ReZG_3}$, $\overline{F}$, $\overline{R}_{-\frac{1}{2}}$, $\overline{SDD}, \overline{H}, \overline{I}, \overline{A}$.

The consistently higher values of TCDs in the HPG structure compared to the RPG suggest that HPG is generally more complex, branched, and/or possesses a greater number of edges for a given size parameter p than RPG. This structural difference can be extrapolated to influence their physicochemical properties: TCDs such as $\overline{M}_1$ and $\overline{M}_2$, which are related to branching and the total π-electron energy, are significantly higher for HPG, suggesting it has greater structural branching and likely a larger effective surface area or molecular complexity. A higher surface area often correlates with enhanced chemical reactivity, better adsorption/catalytic capabilities, and potentially stronger intermolecular forces in HPG compared to RPG. The higher values of $\overline{F}$ and $\overline{A}$ In HPG, which are sensitive to the degree of vertices, suggest a greater contribution from vertices with higher degrees or a more complex overall topology in HPG. These higher TCD values often relate to greater structural stability or higher melting/boiling points within similar compound classes, leading to the suggestion that HPG may exhibit superior thermal or chemical stability compared to RPG. The correlation between TCDs and electronic properties like π-electron energy and the band gap imply that the structural differences highlighted by the TCDs will lead to distinct electronic band structures for HPG and RPG. Consequently, the HPG structure, with its likely greater branching and complexity, might exhibit different conductivity, charge transport, or semiconductor properties compared to the simpler, more linear growth pattern of RPG, making one potentially more suitable for specific electronic or sensor applications than the other.

In summary, the numerical evidence suggests that, beyond the minimal structure, the Hexagonal Porous Graphene (HPG) is structurally more complex and has a higher density of connectivity/branching than the Rectangular Porous Graphene (RPG) for equivalent parameter p. This structural disparity is predicted to translate into HPG having greater surface area, higher reactivity, and potentially enhanced thermal/chemical stability compared to RPG.

4. Discussion

This discussion is structured to first detail the developed quantitative structure–property relationships (Section 4.1). We then address the crucial model limitations and extrapolation uncertainty arising from the small training dataset (Section 4.2), and conclude with a comprehensive agenda for future research aimed at model generalization (Section 4.3).

4.1. The role of topological codescriptors in predicting binding energy

The core achievement of this study is the validation of TCDs derived from the CoM Polynomial as highly accurate and computationally inexpensive predictors for the binding energy of small lithium clusters. The Binding energy measures the energy needed to break the cluster into individual Li atoms, indicating the strength of the interactions maintaining the cluster's integrity, directly influencing the nucleation and growth of lithium dendrites in battery applications. The statistical analysis aimed to determine the optimal structure-property relationship, revealing a significant increase in predictive power upon moving from linear to curvilinear models. Specifically, the Symmetric Division Codescriptor ($\overline{SDD}$) provided a strong linear and quadratic fit with $R^2 = 0.87$ and $R^2 = 0.97$, respectively, while the Randić codescriptor $\overline{R}_{-\frac{1}{2}}$ delivered the highest accuracy via a cubic model $R^2 = 0.99$. This strong correlation confirms that the binding energy is a complex, non-linear function of the cluster's topology, and the CoM Polynomial successfully captures the structural variance necessary to model cluster stability with exceptional fidelity.

4.2. Model limitations and extrapolation

A key limitation of this study is the small dataset used to generate the regression models for binding energy. The models presented in Equations (4)-(6) were trained on only seven data points ($Li_4 - Li_{10}$). This limited size stems from the restricted availability of consistently reported DFT-quality reference data for larger lithium clusters, which are often computationally expensive to model. Therefore, the regression-based expressions in Equations (7) – (8) should be interpreted as preliminary structure–property hypotheses, rather than fully generalized predictive models across all n. For lithium clusters above $n = 10$, the true error band is not yet quantifiable, because no uniform reference dataset exists that spans $n > 10$ Under identical computational conditions. Therefore, a critical direction for future research is the rigorous validation and recalibration of these models; obtaining a harmonized DFT dataset for larger clusters will be essential to enable a full error analysis, refine the curvilinear regression, and confirm whether the observed correlations hold for larger systems.

4.3. Future work

4.3.1. Strengthening and generalizing the lithium cluster framework

Future work will involve a high-level DFT campaign to generate an expanded, harmonized reference dataset for larger lithium clusters (n > 10). This dataset is essential for performing a full quantitative error analysis of the current regression models and for recalibrating the expressions to ensure accurate predictions in the large-n regime. In addition, a systematic study of higher-energy structural isomers (for each n) will be performed to determine whether the present codescriptors can discriminate between small topological variations, which is crucial for accurate modeling of cluster dynamics. The methodology will also be extended to doped lithium clusters (e.g., L_nB, L_nAl). This will test the transferability of the codescriptors to heterogeneous systems and support computational screening of improved anode materials.

Finally, the framework will be expanded to clusters of other alkali metals, particularly sodium and potassium, to evaluate whether the structure–property relationships discovered here are generalizable beyond lithium.

4.3.2. Expanding the structural descriptor family

Future studies should evaluate additional classes of molecular-graph descriptors, including eccentricity-based, reverse-degree, eigenvalue-based, and distance–degree descriptors. The aim is to determine whether these alternative codescriptors yield stronger, less-overfitted correlations with binding energy than those derived from the current CoM Polynomial formulation. The reliability of the codescriptor framework will also be assessed for predicting other fundamental properties, such as bond dissociation energy, fragmentation energy, representative bond-length metrics, and the HOMO–LUMO gap.

4.3.3. Extending the porous graphene topology theory

A final research pillar will generalize the present porous-graphene formulation, which currently treats hexagonal and rectangular motifs, to additional pore geometries such as trapezoidal, rhombic, Kagome, and diamond. Developing these generalized TCD expressions will further demonstrate the versatility of the approach and support the establishment of a unified theory linking pore topology to codescriptor scaling behaviour.

5. Conclusion

The theoretical prediction of material properties, such as the binding energy of lithium clusters, is crucial for understanding the fundamental behavior of materials, optimizing their design, and saving significant time and resources. By guiding experiments into uncharted territory, this approach pushes the boundaries of scientific knowledge.

In this article, we employed codescriptors derived from the CoM Polynomial and curvilinear regression analysis to theoretically predict the binding energy of lithium clusters. Our findings indicate that the Symmetric Division codescriptor is the most effective predictor for both linear and quadratic regression models. For the cubic model, the Randic codescriptor proves to be the superior choice. The statistical validity of these highly significant regression equations is demonstrated in Table 3.

Furthermore, this work extends the CoM Polynomial method to derive generalized analytical expressions for degree-based codescriptors in hexagonal and rectangular porous graphene nanostructures, accompanied by a graphical comparison. We believe the findings presented in this article will facilitate the design of advanced energy storage devices and accelerate the materials discovery cycle.

Acknowledgments: The authors gratefully acknowledge Qassim University, represented by the Deanship of Graduate Studies and Scientific Research, for the financial support for this research under the number (QU-J-UG-2-2025-55724) during the academic year 1446 AH / 2024 AD.

Disclosure Statement

The authors declare that they have no competing interests.

References

[1] Jena, Purusottam, ed. Physics and chemistry of small clusters. Vol. 158. Springer Science & Business Media, 2013.
[2] Saha, Krishnendu, Sarit S. Agasti, Chaekyu Kim, Xiaoning Li, and Vincent M. Rotello. "Gold nanoparticles in chemical and biological sensing." Chemical reviews 112, no. 5 (2012): 2739-2779. https://doi.org/10.1021/cr2001178.
[3] Zhang, Jian, Jiao Li, Yulin Yang, Chuan Yang, Yayu Dong, Kaifeng Lin, Debin Xia, and Ruiqing Fan. "Functionalized rare-earth metal cluster-based materials as additives for enhancing the efficiency of perovskite solar cells." ACS Applied Energy Materials 5, no. 11 (2022): 13318-13326. https://doi.org/10.1021/acsaem.2c01909.
[4] Zheng, Youkun, Lanmei Lai, Weiwei Liu, Hui Jiang, and Xuemei Wang. "Recent advances in biomedical applications of fluorescent gold nanoclusters." Advances in Colloid and Interface Science 242 (2017): 1-16. https://doi.org/10.1016/j.cis.2017.02.005.
[5] Chin, Yu-Cheng, Li-Xing Yang, Fei-Ting Hsu, Che-Wei Hsu, Te-Wei Chang, Hsi-Ying Chen, Linda Yen-Chien Chen et al. "Iron oxide@ chlorophyll clustered nanoparticles eliminate bladder cancer by photodynamic immunotherapy-initiated ferroptosis and immunostimulation." Journal of Nanobiotechnology 20, no. 1 (2022): 373. https://doi.org/10.1186/s12951-022-01575-7.
[6] Mai, Sibei, Jia Sun, Zihan Fang, Guo-Bin Xiao, and Jing Cao. "Metal Clusters Based Multifunctional Materials for Solar Cells." Chemistry–A European Journal (2024): e202303973. https://doi.org/10.1002/chem.202303973.
[7] Fournier, René, Joey Bo Yi Cheng, and Anna Wong. "Theoretical study of the structure of lithium clusters." *The Journal of Chemical Physics* 119, no. 18 (2003): 9444-9454. https://doi.org/10.1063/1.1615237.
[8] Wang, Jinkun, Li Wang, Hong Xu, Li Sheng, and Xiangming He. "Perception of fundamental science to boost lithium metal anodes toward practical application." *Green Energy & Environment* 9, no. 3 (2024): 454-472. https://doi.org/10.1016/j.gee.2023.02.008.
[9] Zhang, Xinyue, Aoxuan Wang, Xingjiang Liu, and Jiayan Luo. "Dendrites in lithium metal anodes: suppression, regulation, and elimination." *Accounts of chemical research* 52, no. 11 (2019): 3223-3232. https://doi.org/10.1021/acs.accounts.9b00437.
[10] Kushwaha, Anoop Kumar, and Saroj Kumar Nayak. "Wobbled electronic properties of lithium clusters: Deterministic approach through first principles." *Physica E: Low-dimensional Systems and Nanostructures* 97 (2018): 368-374. https://doi.org/10.1016/j.physe.2017.12.009.
[11] Brito, B. G. A., Ladir Cândido, JN Teixeira Rabelo, and G-Q. Hai. "Binding energies of small lithium clusters: A comparison of different theoretical calculations." *Chemical Physics Letters* 616 (2014): 212-216. https://doi.org/10.1016/j.cplett.2014.10.044.
[12] Zhou, Kai, Shuwei Wang, Shichao Zhang, Feiyu Kang, and Baohua Li. "Investigating the increased-capacity mechanism of porous carbon materials in lithium-ion batteries." *Journal of materials chemistry A* 8, no. 28 (2020): 14031-14042. https://doi.org/10.1039/D0TA04054A.
[13] Geng, Hongya, Yan Peng, Liangti Qu, Haijiao Zhang, and Minghong Wu. "Structure design and composition engineering of carbon-based nanomaterials for lithium energy storage." *Advanced Energy Materials* 10, no. 10 (2020): 1903030. https://doi.org/10.1002/aenm.201903030.
[14] Qutaish, Hamzeh, Sang A. Han, Yaser Rehman, Konstantin Konstantinov, Min-Sik Park, and Jung Ho Kim. "Porous carbon architectures with different dimensionalities for lithium metal storage." *Science and Technology of Advanced Materials* 23, no. 1 (2022): 169-188. https://doi.org/10.1080/14686996.2022.2050297.
[15] Lee, Jinwoo, Jaeyun Kim, and Taeghwan Hyeon. "Recent progress in the synthesis of porous carbon materials." *Advanced materials* 18, no. 16 (2006): 2073-2094. https://doi.org/10.1002/adma.200501576.

[16] Stein, Andreas, Zhiyong Wang, and Melissa A. Fierke. "Functionalization of porous carbon materials with designed pore architecture." *Advanced Materials* 21, no. 3 (2009): 265-293. https://doi.org/10.1002/adma.200801492.
[17] Wang, Libin, and Xianluo Hu. "Recent advances in porous carbon materials for electrochemical energy storage." *Chemistry–An Asian Journal* 13, no. 12 (2018): 1518-1529. https://doi.org/10.1002/asia.201800553.
[18] Jeong, Jooyoung, Jinyoung Chun, Won-Gwang Lim, Won Bae Kim, Changshin Jo, and Jinwoo Lee. "Mesoporous carbon host material for stable lithium metal anode." *Nanoscale* 12, no. 22 (2020): 11818-11824. https://doi.org/10.1039/D0NR02258F.
[19] Bieri, Marco, Matthias Treier, Jinming Cai, Kamel Aït-Mansour, Pascal Ruffieux, Oliver Gröning, Pierangelo Gröning et al. "Porous graphenes: two-dimensional polymer synthesis with atomic precision." *Chemical communications* 45 (2009): 6919-6921. https://doi.org/10.1039/b915190g.
[20] Li, Bowen, He Xiong, and Yang Xiao. "Progress on synthesis and applications of porous carbon materials." *International Journal of Electrochemical Science* 15, no. 2 (2020): 1363-1377. https://doi.org/10.20964/2020.02.04.
[21] Yang, Tieshan, Han Lin, Xiaorui Zheng, Kian Ping Loh, and Baohua Jia. "Tailoring pores in graphene-based materials: from generation to applications." *Journal of Materials Chemistry A* 5, no. 32 (2017): 16537-16558. https://doi.org/10.1039/C7TA04692H.
[22] Ammon, Maximilian, Tim Sander, and Sabine Maier. "On-surface synthesis of porous carbon nanoribbons from polymer chains." *Journal of the American Chemical Society* 139, no. 37 (2017): 12976-12984. https://doi.org/10.1021/jacs.7b04783.
[23] Su, Chenliang, Muge Acik, Kazuyuki Takai, Jiong Lu, Si-jia Hao, Yi Zheng, Pingping Wu et al. "Probing the catalytic activity of porous graphene oxide and the origin of this behaviour." *Nature communications* 3, no. 1 (2012): 1298. https://doi.org/10.1038/ncomms2315.
[24] Wang, Huan, Xiangjie Bo, and Liping Guo. "Electrochemical biosensing platform based on a novel porous graphene nanosheet." *Sensors and Actuators B: Chemical* 192 (2014): 181-187. https://doi.org/10.1016/j.snb.2013.10.112.
[25] Zhang, Xiong, Haitao Zhang, Chen Li, Kai Wang, Xianzhong Sun, and Yanwei Ma. "Recent advances in porous graphene materials for supercapacitor applications." *Rsc Advances* 4, no. 86 (2014): 45862-45884. https://doi.org/10.1039/C4RA07869A.
[26] Huang, Haibo, Haodong Shi, Pratteek Das, Jieqiong Qin, Yaguang Li, Xiao Wang, Feng Su et al. "The chemistry and promising applications of graphene and porous graphene materials." *Advanced Functional Materials* 30, no. 41 (2020): 1909035. https://doi.org/10.1002/adfm.202070275.
[27] Balaban Alexandru T., and James Devillers, eds. *Topological indices and related descriptors in QSAR and QSPAR*. CRC Press, 2014.
[28] Trinajstic, Nenad. *Chemical graph theory*. Routledge, 2018. https://doi.org/10.1201/9781315139111.
[29] Wiener, Harry. "Correlation of heats of isomerization, and differences in heats of vaporization of isomers, among the paraffin hydrocarbons." *Journal of the American Chemical Society* 69, no. 11 (1947): 2636-2638. https://doi.org/10.1021/ja01203a022.
[30] Deutsch, Emeric, and Sandi Klavžar. "M-polynomial and degree-based topological indices." *Iran J. Math. Chem.,* 6 (2) (2015), pp. 93-102
[31] Mondal, Sourav, Nilanjan De, and Anita Pal. "On some new neighbourhood degree based indices." *Acta Chemica Iasi*, 27 (1) (2019), pp. 31-46. https://doi.org/10.2478/achi-2019-0003.
[32] Kirmani, Syed Ajaz K., and Parvez Ali. "CoM polynomial and topological coindices of hyaluronic acid conjugates." *Arabian Journal of Chemistry* 15, no. 7 (2022): 103911. https://doi.org/10.1016/j.arabjc.2022.103911.
[33] Albadrani, Mohammed, Parvez Ali, Waleed H. El-Garaihy, and Hassan Abd El-Hafez. "Prediction of Exchange-Correlation Energy of Graphene Sheets from Reverse Degree-Based Molecular Descriptors with Applications." *Materials* 15, no. 8 (2022): 2889. https://doi.org/10.3390/ma15082889.
[34] Shanmukha, M. C., A. Usha, K. C. Shilpa, and N. S. Basavarajappa. "M-polynomial and neighborhood M-polynomial methods for topological indices of porous graphene." *The European Physical Journal Plus* 136 (2021): 1-16. https://doi.org/10.1140/epjp/s13360-021-02074-8.
[35] Govardhan, S., and S. Roy. "Topological analysis of hexagonal and rectangular porous graphene with applications to predicting-electron energy." *The European Physical Journal Plus* 138, no. 7 (2023): 670. https://doi.org/10.1140/epjp/s13360-023-04307-4.
[36] Krishnan, Sathish, and Bharati Rajan. "Molecular descriptor analysis of polyphenylene superhoneycomb networks." *Polycyclic Aromatic Compounds* 43, no. 5 (2023): 4803-4815. https://doi.org/10.1080/10406638.2022.2094972.
[37] Aftab, Muhammad Haroon. "Measuring irregularities in the chemical compound: porous graphene." *Polycyclic Aromatic Compounds* (2023): 1-10.
[38] Balasubramanian, Krishnan. "Density functional and graph theory computations of vibrational, electronic, and topological properties of porous nanographenes." *Journal of Physical Organic Chemistry* 36, no. 12 (2023): e4435. https://doi.org/10.1002/poc.4435.
[39] Chetri, Pawan, Ramesh Ch Deka, and Amarjyoti Choudhury. "Structural and electronic properties of Lin (n= 2–10) clusters: A density functional study." *Physica B: Condensed Matter* 430 (2013): 74-80. https://doi.org/10.1016/j.physb.2013.08.005.
[40] Chetri, Pawan, Bijit Bora, and Tapan Kumar Baishya. "Molecular graph theory based study on Lin cluster: a correlation between physical property and topological descriptors." *Bulletin of Materials Science* 44, no. 3 (2021): 212. https://doi.org/10.1007/s12034-021-02500-8.
[41] Berhe, Melaku, and Chunxiang Wang. "Computation of certain topological coindices of graphene sheet and () nanotubes and nanotorus." *Applied Mathematics and Nonlinear Sciences* 4, no. 2 (2019): 455-468. https://doi.org/10.2478/AMNS.2019.2.00043.
[42] Ali P, Alhabib OM, AlSulaim SK. Prediction of cluster energy of lithium clusters from codescriptors with application in 2D porous graphene. Advances in Mechanical Engineering. 2024;16(9). https://doi.org/10.1177/16878132241282933.